AAS 17-312

NEW PRACTICAL RESULTS FOR FLAT-SPIN RECOVERY BY EQUATORIAL TORQUES

Frank L. Janssens[1] and Jozef C. Van der Ha[2]

The paper studies the motion of a spinning rigid asymmetric body under an equatorial torque (i.e., normal to spin axis). Through extensive simulations, starting from pure flat-spin motion, four types of motion are identified and visualized as zones within the plane formed by the two torque components. The zone "No Recovery" describes a new type of unstable motion. The zone "Slow flat spin recovery" gives new insights into the efficiency of a recovery strategy by an equatorial torque. For the zone "Fast Recovery" a new approximate analytical model involving Fresnel integrals has been established for modeling the asymptotic rotational motion.

INTRODUCTION

The recovery from a flat-spin motion is one of the most remarkable practical applications in the field of spinning-satellite dynamics. Following up on our previous work in this field[1,2], we present here new practical results for the flat-spin recovery by means of a constant body-fixed torque. We consider a spinning rigid asymmetric body subjected to a torque that acts in a plane perpendicular to the axis of maximum inertia. We refer to an *equatorial* torque in this case. The initial conditions that are studied in this paper are those of a *pure* spin about the maximum axis of inertia. The presence of a residual nutation about the maximum axis increases the number of free parameters and the phase angle at the start of the maneuver plays a role as well. A few qualitative features of the impact of the nutation phase angle will be addressed.

The dynamical model is a special case of the 'self-excited rigid body' problem which has a rich history[3-9]. It is the simplest possible extension of a free rigid body with constant body-fixed torque components on the right-hand sides of the Euler equations. A complete solution for all possible initial conditions, inertias, and torques would have 9 independent parameters. Therefore, it is no surprise that solutions are available only in a limited part of this parameter space. In this paper, we consider the families of solutions that are parameterized in two torque components while taking the third component zero.

The two most important applications of this problem for satellite applications are: i) motion resulting from a fail-open of an attitude control thruster; ii) motion during a flat-spin recovery operation. Flat-spin refers to a spacecraft that was initially spinning about its *minimum* axis of inertia but, because of energy-dissipation effects, ended up spinning about its *maximum* axis of inertia. The purpose of a flat-spin recovery strategy is to re-establish the original spin about the *minimum*-inertia axis. This corresponds to the typical orientation for performing large orbit-injection burns. A recovery strategy that uses only one thruster in a continuous-thrust mode is the most attractive because of its simplicity.

[1] Consultant, Wilhelminastraat 29, 2201 KA Noordwijk, the Netherlands; f.janssens@ziggo.nl.
[2] Consultant, 5808 Bell Creek Rd, Deming, WA 98244, USA; jvdha@aol.com.

A pioneering paper about flat-spin recovery is Barba et al.[10], who conclude that a torque about the minimum axis must exceed a critical value to make the recovery feasible. However, their value for the critical torque was too low because of the adoption of a symmetrical satellite model. Their analyses and numerical simulations illustrate the practical implementation aspects very well. Cronin[11] derives the correct value for the critical torque for an asymmetric body and based on the initial conditions of a pure flat-spin. Livneh and Wie[12,13] obtain the same result in modern terminology and present complete results for the effects of torques on any of the principal axes.

In a recent paper, Manchester[14] presents nonlinear Lyapunov-based feedback control laws (for reaction wheels) driving a spinning spacecraft from any initial state to a minor-axis spin. The controllers provide almost-global asymptotic stability and can accommodate actuator limits.

After introducing the mathematical basis of the model, this paper pursues two main objectives. First, we present the results of extensive numerical simulations that provide valuable new insights into the practical implementation of a flat-spin recovery strategy. In particular, we provide a summary Figure that categorizes the different types of motion resulting from an equatorial torque acting on a spacecraft that is initially in flat-spin motion. The two free parameters are the equatorial torque components T_1 and T_2 (about the minimum and intermediate axes of inertia, respectively). A first observation is that the types of solutions are not continuous across the boundaries between the zones.

These results also provide valuable new insights for a flat-spin recovery strategy based on simply switching on an equatorial torque. In contrast to a torque about the minimum axis the gyroscopic coupling guarantees a recovery if the equatorial torque has a *negative* component about the intermediate axis of inertia. Naturally, the recovery time increases with decreasing torque magnitude. However, if the torque magnitude is below the critical value mentioned above, the transition to a spin about the minimum axis occurs already during the first nutation revolution. Furthermore, the residual nutation at the end of the maneuver is reduced as well.

Finally, the last part of the paper presents new compact approximate analytical solutions for modeling the motion of a flat-spin recovery strategy by an equatorial torque.

FUNDAMENTALS OF ROTATIONAL MOTION

Euler Equations

We study the motion of an asymmetrical (i.e., triaxial) spinning rigid body under an external torque vector **T** with, in general, constant non-zero components T_j (j = 1, 2, 3) about the three principal body axes. This is a continuation of our previous work[1,2] on flat-spin recovery and on self-excited rigid-body dynamics in general[7,8].

The rotation rates governing the attitude motion obey the well-known Euler equations, which describe the rotational motion within a principal body reference frame:

$$\begin{aligned} A\,\dot{\omega}_1 + (C-B)\,\omega_2\,\omega_3 &= T_1 \\ B\,\dot{\omega}_2 - (C-A)\,\omega_1\,\omega_3 &= T_2 \\ C\,\dot{\omega}_3 + (B-A)\,\omega_1\,\omega_2 &= T_3 \end{aligned} \qquad \text{(1a-c)}$$

The dots denote time-derivatives and ω_j (j = 1, 2, 3) are the components of the rotation vector $\boldsymbol{\omega}$ along the principal x, y, z body axes, respectively. The parameters A, B, C refer to the principal moments of inertia along these axes in an increasing sequence:

$$A < B < C \qquad (2)$$

Equality of any two of the principal inertias is excluded here because these cases require different analyses.

We introduce the inertia coefficients:

$$k_1 = (C-B)/A; \quad k_2 = (C-A)/B; \quad k_3 = (B-A)/C \tag{3a-c}$$

which satisfy $0 < k_j < 1$ for $j = 1, 2, 3$. Also we define $m_j = T_j / I_j$ in units of $1/s^2$, where I_j are the moments of inertia along the x_j axis ($j = 1, 2, 3$). Eqs. (1) become now:

$$\begin{aligned} \dot{\omega}_1 + k_1 \omega_2 \omega_3 &= m_1 \\ \dot{\omega}_2 - k_2 \omega_1 \omega_3 &= m_2 \\ \dot{\omega}_3 + k_3 \omega_1 \omega_2 &= m_3 \end{aligned} \tag{4a-c}$$

A spinning satellite that is in a *pure* flat-spin motion about the major inertia axis (i.e., z-axis) at time t_0 has the following initial rotation rates about the principal axes:

$$\omega_1(t_0) = \omega_{10} = 0; \quad \omega_2(t_0) = \omega_{20} = 0; \quad \omega_3(t_0) = \omega_{30} = \Omega_0 > 0 \tag{5a-c}$$

Finally, we introduce the (flat-spin) nutation frequency ω_n, which is defined by:

$$\omega_n = k\,\Omega_0 \quad with: \quad k = \sqrt{k_1 k_2} = \sqrt{\frac{(C-B)(C-A)}{AB}} \tag{6a,b}$$

Approximate Rotational Model for $m_3 = 0$

Here we consider the case $m_3 = 0$. Eqs. (4,5) may be solved in terms of Taylor expansions in powers of t (Appendix A). This shows that the spin rate may be taken constant, at least initially:

$$\omega_3(t) = \Omega_0 - \frac{k_3}{3} m_1 m_2 t^3 + O(t^4) \cong \Omega_0 \tag{7}$$

We introduce the *complex* representation of the scaled equatorial rate components:

$$\boldsymbol{w}(t) = \frac{\omega_1}{\sqrt{k_1}} + j\frac{\omega_2}{\sqrt{k_2}}; \quad \boldsymbol{\mu} = \frac{m_1}{\sqrt{k_1}} + j\frac{m_2}{\sqrt{k_2}} \tag{8}$$

where j denotes the complex unit. After this scaling Eqs. (4a,b) can be written in the same form as for a symmetrical body ($A = B \Rightarrow k_1 = k_2$):

$$\dot{\boldsymbol{w}}(t) - j\omega_n \boldsymbol{w}(t) = \boldsymbol{\mu} \tag{9}$$

with initial condition $\boldsymbol{w}(0) = 0$ from Eqs. (5a,b). The solution of Eq. (9) is given by:

$$\boxed{\boldsymbol{w}(t) = j\frac{\boldsymbol{\mu}}{\omega_n}\left\{1 - e^{j\omega_n t}\right\}} \tag{10}$$

The explicit solutions for the components of $\boldsymbol{w}(t)$ can be written as:

$$\begin{pmatrix} w_1(t) \\ w_2(t) \end{pmatrix} = \frac{1}{\omega_n}\begin{bmatrix} s(t) & c(t)-1 \\ 1-c(t) & s(t) \end{bmatrix}\begin{pmatrix} \mu_1 \\ \mu_2 \end{pmatrix} \tag{11}$$

with:

$$s(t) = \sin(\omega_n t); \quad c(t) = \cos(\omega_n t) \tag{12a,b}$$

The results in terms of the equatorial angular rates $\omega_1(t)$ and $\omega_2(t)$ are:

$$\omega_1(t) = \omega_{1C} + \frac{\sqrt{k_1}}{\omega_n}\left\{\mu_1 \sin(\omega_n t) + \mu_2 \cos(\omega_n t)\right\} \tag{13a}$$

$$\omega_2(t) = \omega_{2C} + \frac{\sqrt{k_2}}{\omega_n}\left\{\mu_2 \sin(\omega_n t) - \mu_1 \cos(\omega_n t)\right\} \tag{13b}$$

with:

$$\omega_{1C} = -\frac{\sqrt{k_1}\mu_2}{\omega_n} = -\frac{T_2}{(C-A)\Omega_0}; \quad \omega_{2C} = \frac{\sqrt{k_2}\mu_1}{\omega_n} = \frac{T_1}{(C-B)\Omega_0} \tag{14a,b}$$

The nutation frequency ω_n remains constant because the spin rate Ω_0 is taken constant.

The results of Eqs. (13) indicate that the equatorial rates describe an ellipse with center at point C = (ω_{1C}, ω_{2C}). The semi-major axis of the ellipse corresponds to the intermediate axis of inertia and the semi-minor axis is along the minimum axis of inertia. The ellipse's eccentricity is equal to $\sqrt{(1-k_1/k_2)}$, which depends only on the moments of inertia and is not affected by the torque or spin rate. Figures 1a,b show these ellipses for two cases with identical torques about the x-axis but opposite torques about the y-axis (and input inertias A = 200; B = 300; C = 400 kgm^2).

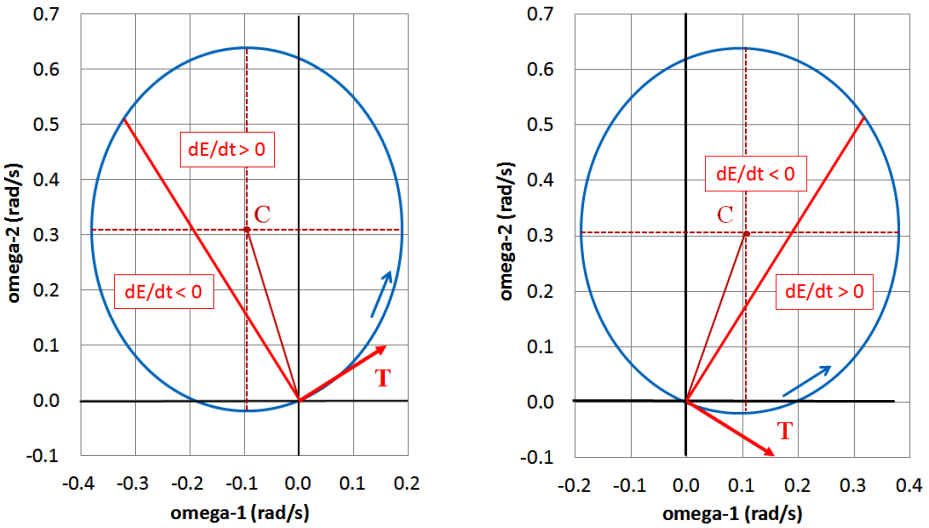

(a) T_2 = 10 Nm **(b) T_2 = -10 Nm**

Figures 1 - Trajectories of ω_1, ω_2 for T_1 = 16.22 Nm and Opposite T_2 Components.

It is easy to see that the harmonic functions $\sin(\omega_n t)$, $\cos(\omega_n t)$ in Eqs. (13a,b) average out to zero over the ellipse. Therefore, the average values of $\omega_1(t)$ and $\omega_2(t)$ during the nutation period may be approximated by the constants ω_{1C} and ω_{2C}, respectively. These average rates are useful for calculating the average changes in the energy and in the square of the modulus of the angular momentum over the ellipse. Starting from the well-known instantaneous relationships, see for instance Eqs. (8) of Ref. 2:

$$\frac{d}{dt}\left\{E(t)\right\} = \boldsymbol{\omega}\bullet\mathbf{T}; \quad \frac{1}{2}\frac{d}{dt}\left\{H^2(t)\right\} = \mathbf{H}\bullet\mathbf{T} \tag{15a,b}$$

and replacing the relevant entries by their respective averages, we find:

$$\frac{d}{dt}\langle E(t)\rangle = \omega_{1C}T_1 + \omega_{2C}T_2 = \frac{k_3 C m_1 m_2}{k^2 \Omega_0} \tag{16a}$$

$$\frac{1}{2}\frac{d}{dt}\langle H^2(t)\rangle = A\,\omega_{1C}T_1 + B\,\omega_{2C}T_2 = \frac{k_3 C^2 m_1 m_2}{k^2 \Omega_0} \tag{16b}$$

where <…> denotes the averaging operation over the nutation period.

Now we introduce the slowly-varying quantity $\Omega(t) = <\omega_3(t)>$ in $H(t) = C\,\Omega(t)$ since initially $H_0 = C\Omega_0$. Thus, Eq. (16b) produces a first-order differential equation for $\Omega(t)$:

$$\Omega^2(t)\,\dot{\Omega}(t) \cong \frac{k_3 m_1 m_2}{k^2} \tag{17}$$

with solution:

$$\Omega(t) \cong \Omega_0\left(1+\frac{t}{\tau}\right)^{1/3} \quad with: \quad \tau = \frac{k^2\Omega_0^3}{3k_3 m_1 m_2} \tag{18a,b}$$

Eqs. (18) show that the average value of $\omega_3(t)$ increases or decreases according to the sign of the product $T_1 T_2$. In fact, the domain of validity of this approximation turns out to be larger than expected a priori for the combination $T_1 > 0$, $T_2 < 0$, see example in Fig. 1c.

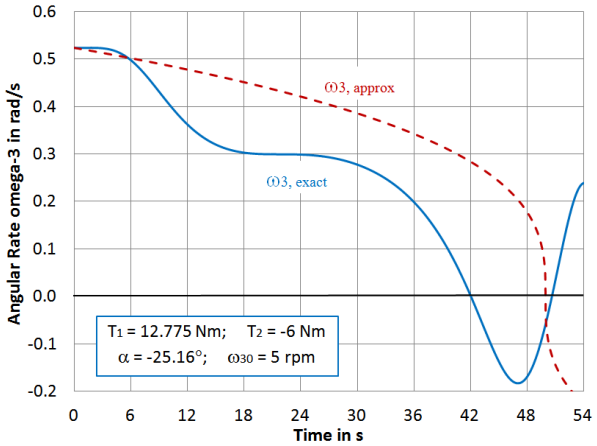

Figure 1c - Comparison of $\omega_3(t)$ and $\Omega(t)$.

Eqs. (18) have previously been derived by the authors[7,8] using different approaches.

Useful Quantities

The two well known first integrals of force-free motion are the rotational energy E and the modulus of the angular momentum H. In the presence of a body-fixed torque they become functions of time:

$$E(t) = \frac{1}{2}\left(A\omega_1^2 + B\omega_2^2 + C\omega_3^2\right); \quad H^2(t) = A^2\omega_1^2 + B^2\omega_2^2 + C^2\omega_3^2 \tag{19a,b}$$

When the body-fixed torque acts about one of the principal axes of inertia there exists, for each specific case, a linear combination of E and H^2 that is a first integral:

a) Torque on the minimum axis (A):

$$\Delta E_{max}(t) = \frac{H^2(t)}{2A} - E(t) = \frac{BC}{2A}\left(k_3\omega_2^2 + k_2\omega_3^2\right) \geq 0 \tag{20a}$$

b) Torque on the intermediate axis (B):

$$\Delta E_{sep}(t) = \frac{H^2(t)}{2B} - E(t) = \frac{AC}{2B}\left(k_1\omega_3^2 - k_3\omega_1^2\right) \geq or \leq 0 \tag{20b}$$

c) Torque on the maximum axis (C):

$$\Delta E_{min}(t) = E(t) - \frac{H^2(t)}{2C} = \frac{AB}{2C}\left(k_2\omega_1^2 + k_1\omega_2^2\right) \geq 0 \tag{20c}$$

For a given value of angular momentum, ΔE_{max} (ΔE_{min}) is the deficit (excess) between the current value of the energy and its maximum (minimum) value. The sign of ΔE_{sep} determines whether the motion is about the maximum or minimum axis of inertia.

The three quantities defined in Eqs. (20) appear also in the constants of the formulae describing the force-free motion (see Ref. 15) when all initial conditions are considered. Their rates of change under a *general* torque follow from Eqs. (20) with help of Eqs. (15):

$$\frac{d}{dt}\left\{\Delta E_{max}(t)\right\} = \frac{BC}{A}\left\{k_3 m_2 \omega_2 + k_2 m_3 \omega_3\right\} \tag{21a}$$

$$\frac{d}{dt}\left\{\Delta E_{sep}(t)\right\} = \frac{AC}{B}\left\{k_1 m_3 \omega_3 - k_3 m_1 \omega_1\right\} \tag{21b}$$

$$\frac{d}{dt}\left\{\Delta E_{min}(t)\right\} = \frac{AB}{C}\left\{k_2 m_1 \omega_1 + k_1 m_2 \omega_2\right\} \tag{21c}$$

In the case of an equatorial torque all these combinations are time dependent. The results of Eqs. (21) reveal which quantity is conserved when a single torque component is acting. The two most important results for a flat-spin recovery under an equatorial torque are:

$$\frac{d}{dt}\left\{\Delta E_{max}(t)\right\} = \frac{BC}{A} k_3 m_2 \omega_2 \tag{22a}$$

$$\frac{d}{dt}\left\{\Delta E_{sep}(t)\right\} = -\frac{AC}{B} k_3 m_1 \omega_1 \tag{22b}$$

Eqs. (22) show that the signs of the rates of change of ΔE_{max} and ΔE_{sep} depend not only on the torque components m_2 and m_1 but, due to the gyroscopic coupling, also on the products $\omega_2 m_2$ and $\omega_1 m_1$, respectively. Later on it will become clear that the sign changes of these products are important for determining the types of the solutions.

The smaller ΔE_{max} is, the closer we approach a pure spin motion about the minimum axis. During a flat-spin recovery, the value of ΔE_{sep} starts out positive and turns negative at the crossing of the separatrix, which is the transition to the spin about the minimum axis.

RESULTS OF NUMERICAL SIMULATIONS

Classification of Types of Motion

Figure 2 summarizes the numerical results for an equatorial torque acting on a body that, initially, is spinning about its maximum axis of inertia. The two free parameters are the equatorial torque components T_1 and T_2 (about the minimum and intermediate axis of inertia, respectively). Both are switched on simultaneously at $t = 0$. We consider only the case $T_1 > 0$ which is required to establish a *positive* spin about the minimum-inertia axis.

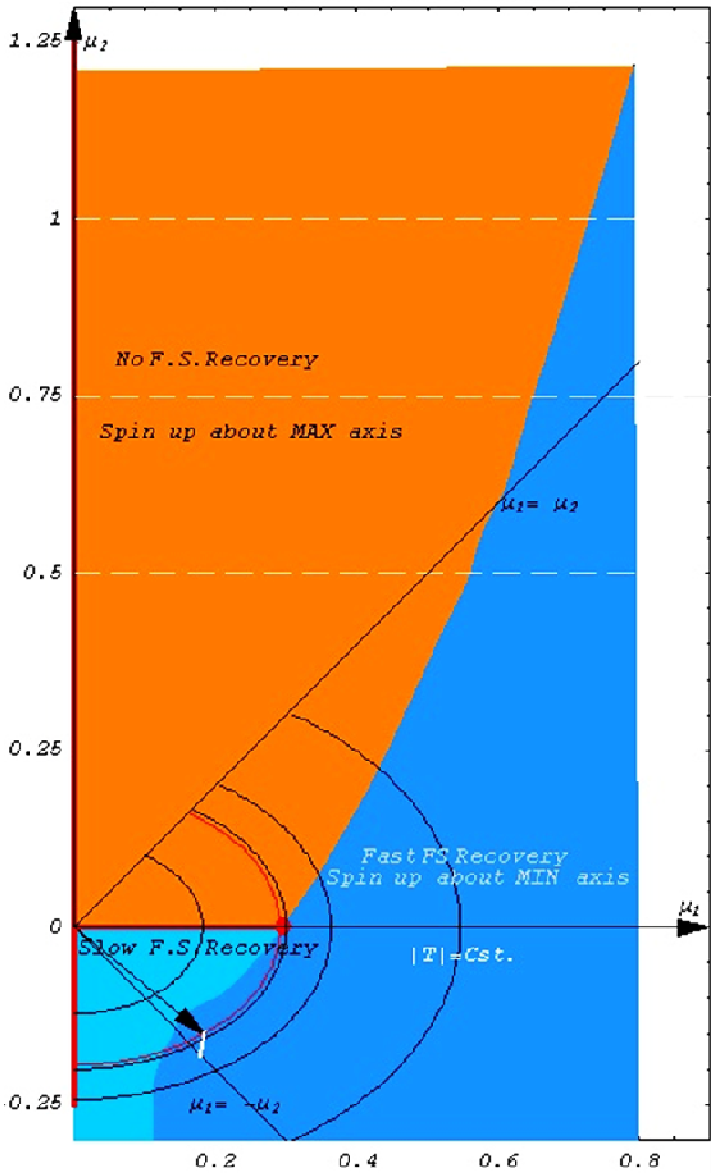

Figure 2 - Summary of Flat-Spin Recovery by Equatorial Torque ($T_1 > 0$, any T_2).

The axes of Fig. 2 represent special cases when only *one* torque component is active. The *x* and *y* axes stand for the parameters $\mu_1 = m_1/\Omega_0^2$ and $\mu_2 = m_2/\Omega_0^2$, respectively. We may interpret m_j (j = 1, 2) as the rate of change of the angular velocity or the slope of the linear growth of ω_j starting from zero and T_j the only active torque component. Another interpretation of m_j is that of a frequency squared which makes μ_j the ratio of two squared frequencies. Thus, μ_j measures the weight of a torque component relative to the initial spin rate squared.

Torque on a Single Axis (Intermediate or Minimum)

When $T_2 = 0$ the torque acts on the minimum principal axis. Eq. (22a) shows that the quantity ΔE_{max} is conserved in this case. The solutions are periodic about the (initial) maximum-inertia axis if T_1 is below a critical value T^*. Figure 4 of Ref. 2 shows that the critical value T^* follows from the requirement that, at the time t_1 when the angular velocity $\omega_1(t)$ reaches its first minimum, i.e. $\dot{\omega}_1(t_1) = 0$, also $\omega_1(t_1)$ must vanish. From Eqs. (25-27) of Ref. 2 we find:

$$\mu_1^* = \frac{k_1}{2}\sqrt{\frac{k_2}{k_3}}\sin(2u^*) \quad with: \quad \tan(u^*) = \frac{1}{\pi - (2u^*)} \tag{24a,b}$$

Figure 10a in Ref. 2 shows the angular rates with their elongated periods when T_1 approaches the critical value from below. Their values hover very close to an unstable stationary solution ($u^* \approx 23.2°$, Fig. 6 in Ref. 2). When $T > T^*$, the first minimum occurs during the *first* revolution after activation of the torque. We call this type of recovery a 'Fast Recovery' in Fig. 2. The mathematical model is a generalized rotating pendulum.

The red dot in Fig. 2 identifies $T_1 = T^*$ and the red line segment indicates the periodic solutions. The case $T_2 = 0$ offers an intuitive dynamical model for flat-spin recovery and has been studied by Barba et al.[10] and Cronin[11].

On the vertical axis of Fig. 2 only the torque component T_2 about the *intermediate* principal axis is active (as $T_1 = 0$). In this case, Eq. (21b) shows that ΔE_{sep} is a first integral. From Eq. (20b) follows then that $\{\omega_3, \omega_1\}$ describe segments of a hyperbola during the motion. A similar analysis as was done in Ref. 2 for ΔE_{max} (harmonic functions for ω_2, ω_3) shows that ω_3 never changes sign. The solution is always a periodic motion about the maximum axis since $\Delta E_{sep} > 0$ for $\omega_{10} = 0$ (see Eq. 20b) during the motion.

The fact that periodic solutions exist only *on* the axes has consequences for the feasibility of techniques like 'Variation of Parameters' when extending the solutions into the plane. The slightest excursion away from the axis changes the nature of the solutions, which violates the implicitly assumed continuity of a perturbation method.

Both Torque Components Non-zero and $T_2 > 0$

Here we analyze what happens to the periodic solutions when *both* torque components are non-zero. When starting with $T_2 > 0$ and moving into the first quadrant in Fig. 2, with $T_1 < T^*$, we find that there is no flat-spin recovery in the orange zone.

Figure 3 shows the slow spin-up about the *maximum* axis that occurs in this zone. The amplitudes of ω_1 and ω_2 increase faster than the increase in spin rate. If the torque remains active, all three angular rate components approach infinity asymptotically. (In case of a thruster-open failure, this situation would imply a catastrophic end-of-mission scenario!)

Nevertheless, critical values $T^{*\prime}$ (i.e., the border between the orange and dark blue zones in Fig. 2) still exist for any $T_2 > 0$ where the value of $T^{*\prime}$ increases as a function of T_2. This confirms that flat-spin recoveries do in fact occur for $T_2 > 0$. This is in contrast with the *approximate* result in Eqs. (18), which predict that a flat-spin recovery would not be possible in the full first quadrant because result $\omega_3(t)$ would keep increasing for any $T_2 > 0$. When studying cases with non-zero initial nutation in Ref. 2 we found that an initial condition $\omega_{20} > 0$ leads to an increase in the value of T^*. Likewise, a positive torque T_2 produces $\omega_2(t) = m_2 t > 0$ initially. Thus, both cases require a larger torque T_1 to achieve a recovery.

The transition (i.e., flat-spin recovery) to the minimum axis is also guaranteed if the first minimum of $\omega_1 \geq 0$, exactly as in the case $T_2 = 0$. However, in case $T_2 > 0$, the values $T^{*\prime}$ cannot be obtained analytically. Since $m_2 > 0$ and $\omega_2(t) \approx m_2 t$, the product $m_2 \omega_2(t) > 0$ and Eq. (22a) indicates that $\Delta E_{max}(t)$ increases initially. After the recovery, however, it stabilizes on a constant value. A typical evolution of ΔE_{max} will be shown in Fig. 5b below.

The Figures presented in this paper originate from dynamical simulations that employ the following moments of inertia: $A = 200$, $B = 300$, $C = 400$ kg m^2, respectively.

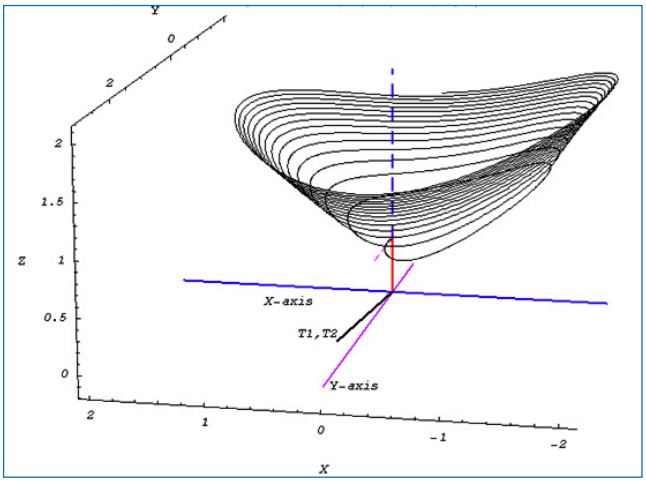

Figure 3 - Rotation Vector $\boldsymbol{\omega}(t)$ in Body Frame for $T_1 = 10$; $T_2 = 100$ Nm and $\omega_{30} = 5$ rpm.

Both Torque Components Non-zero and $T_2 < 0$

In Ref. 1 we established that a transition to a spin about the minimum axis always occurs if the torque vector is in the fourth quadrant $\{T_1 > 0, T_2 < 0\}$. It turns out that $T_2 < 0$ splits up in several cases with important consequences for the flat-spin recovery. As mentioned above, the negative T_2 axis as well as the segment $[0, T^*]$ of the T_1 axis are excluded (as they have periodic solutions). For any point inside this quadrant a transition to a spin-up about the minimum axis can be guaranteed. Eq. (18a) shows that, in average, ω_3 decreases during a complete revolution about the maximum axis of inertia. This is not true for a symmetrical (i.e., $A = B$) body, which has other types of transitions.

The curve that separates the recovery zone (blue) from the non-recovery zone (orange) in the first quadrant continues in the 4th quadrant and '*Fast* Recoveries' continue to exist to the right of this curve. A fast recovery is now achieved with a smaller critical value $T^{*\prime} < T^*$ (i.e., dark blue zone in the 4th quadrant of Fig. 2). The light blue zone in Fig. 2 refers to a '*Slow Recovery*' because the transition is not achieved during the first revolution.

When approaching the T_1 axis ($T_2 \rightarrow 0$), the recovery starts with a phase during which periodically $\omega_1(t) < 0$. It may take a long time before the first positive minimum of ω_1 occurs (at $t \approx 95$ s in Fig. 4a). When approaching the T_2 axis ($T_1 \rightarrow 0$), $\omega_1(t) > 0$ from the start but the transition to the minimum axis occurs much later (see Fig. 4b). Likewise, the crossings of $\omega_3 = 0$ occur at $t \approx 105$ *s* in Fig 4a and much later, at $t > 300$ *s*, in Fig. 4b.

We note that the transition to a spin about the minimum axis in Fig. 4b occurs only when the spin rate ω_3 has decreased sufficiently in average value. Due to its initial non-zero flat-spin rate, $\omega_3(t)$ behaves as if a negative T_3 is acting. A recovery procedure that combines, simultaneously or sequentially, $T_3 < 0$ and $T_1 > 0$ is in fact the most intuitive approach for a flat-spin recovery procedure. The results indicate that the gyroscopic coupling effect ensures that a torque $T_2 < 0$ may induce the same effect.

Figure 5a illustrates the evolution of $\Delta E_{max}(t)$ for the case $T_1 > 0$, $T_2 < 0$. Its value decreases rapidly from the initial 54.83 Nm and eventually ends up oscillating about the asymptotic value $\Delta E_{max}(\infty) \approx 21$ Nm. The smaller the value of $\Delta E_{max}(t)$ is, the closer the energy $E(t)$ is to the maximum possible value that is compatible with the angular momentum (see Eq. 20a). Furthermore, as a consequence, the smaller also the residual nutation will be. In this sense, the flat-spin recovery illustrated in Fig. 5a is superior to the recovery shown in Fig. 5b.

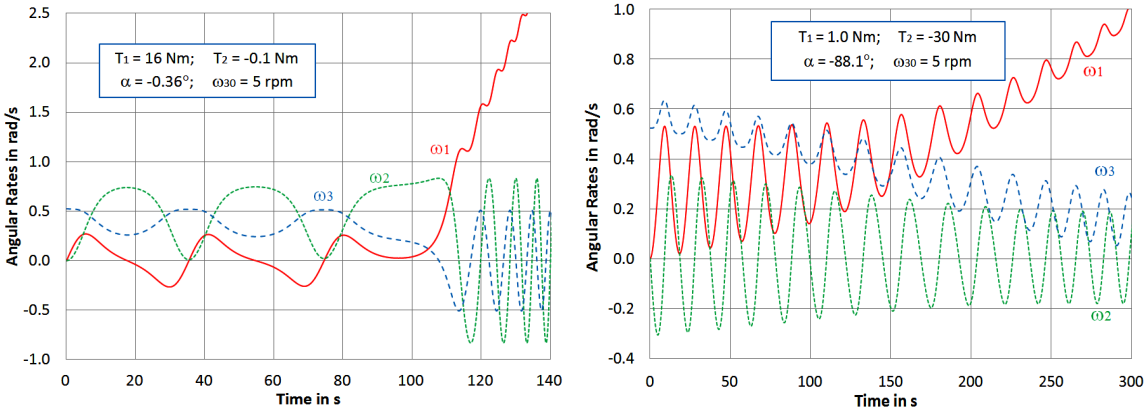

(a) **(b)**

Figures 4 – Examples of Slow Recoveries: a) Close to T_1 Axis; b) Close to T_2 Axis.

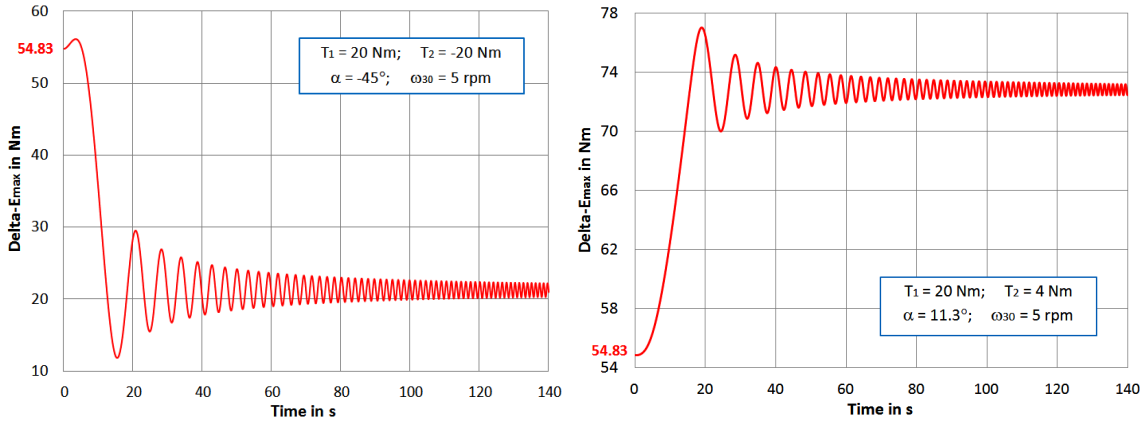

(a) **(b)**

Figures 5 – a) Case $T_2 < 0$; $\Delta E_{max}(\infty) < \Delta E_{max}(0)$; b) Case $T_2 > 0$; $\Delta E_{max}(\infty) > \Delta E_{max}(0)$.

Summary of Classifications

For an initial spin about the maximum axis we distinguish the following cases:

a) Periodic solutions occur only for *single-axis* torque: $T_1 < T^*$ (x-axis) or any T_2 (y-axis).

b) For the combination $\{T_1, T_2\}$, there exists for *any* T_2 a $T^{*\prime}$ such that, when $T_1 > T^{*\prime}$, a switch-over to a spin-up about the minimum axis of inertia takes place during the first revolution. While the spin-up about the minimum axis continues, the path of (ω_3, ω_2) converges to an ellipse with constant axes. The global motion stays on an elliptical cylinder with axis in the direction of T_1.

c) When $T_1 < T^*$ and $T_2 > 0$, the motion remains spinning about the maximum axis with all three components diverging to infinity (see Fig. 3).

d) When $T_1 < T^*$ and $T_2 < 0$, a transition to a spin about the minimum axis will always take place but is preceded by a decrease of the rate ω_3 (see Figs. 4a,b).

e) After the transition to a spin about the minimum axis, the average increase of ω_1 occurs at the rate m_1 (see Figs. 7a,b). This is in agreement with Eq. (4a) under the condition that the product term $<\omega_2\, \omega_3>$ averages to zero.

APPLICATION OF FLAT-SPIN RECOVERY WITH $T_2 < 0$

Ref. 1 shows that $T_2 < 0$ is a *sufficient* condition for a flat-spin recovery. The interesting result here is that a fast recovery can take place with $|\mathbf{T}| < T^*$ by selecting the thruster such that the component T_2 is negative. This is illustrated for $\mathbf{T}$ = [10, -10] (i.e., green dot in Fig. 6) with modulus $|\mathbf{T}|$ = 14.14 Nm, which is smaller than T^* = 16.2203 Nm (i.e., red dot in Fig. 6).

The results are visualized in Figs. 7a,b. These Figures contain straight lines with slope m_1 which match the average increases of ω_1 after the recovery. Such lines exist for any (fast or slow) type of recovery. The time t_0 at which this line crosses its zero value cannot be determined a priori with sufficient accuracy in all cases.

The first column of Table 1 contains the various characteristic times of the recovery's progress for the two cases shown in Figs. 7a,b. The first row gives the time when ω_1 reaches its minimum of (theoretically) zero and remains positive from there onwards. This value can be computed analytically (see Ref. 2, Eq. 27) and implies that the recovery will occur at a later time when the vector $\boldsymbol{\omega}$ crosses the separatrix.

Figure 7b shows an earlier time for the first (non-zero!) minimum of ω_1 than Fig.7a. This is a consequence of the gyroscopic coupling induced by T_2. Lines 2-4 of Table 1 show that also the actual recovery ($\Delta E_{sep} = 0$), as well as the time when ω_3 turns negative, occur earlier for the case in Fig. 7b. It was not necessary to investigate these events in the analysis of a recovery with $T_2 = 0$ in Ref. 2 since all information could be deduced from the analytic solution $\omega_1(t)$. Line 5 of Table 1 gives the time t_s from which the averaged linear solution for $\omega_1(t) = m_1(t - t_s)$ is valid.

Finally, the last two rows recapitulate the initial and final values of ΔE_{max} (i.e., the difference between actual and maximum possible value of the rotational energy that is compatible with the actual angular momentum). In the case $T_2 = 0$ (Fig. 7a) ΔE_{max} remains constant throughout the simulation. On the other hand, when $T_2 < 0$ (Fig. 7b) ΔE_{max} varies considerably over time and converges to a low asymptotic value as shown in Fig. 8.

The asymptotic value is reached for the first time at 51.34 *s*. As in Figs. 5, a smaller value of ΔE_{max} implies that the motion is closer to the axis of minimum energy. Hence, the nutation is smaller and the amplitudes of the transverse rates ω_2 and ω_3 are smaller as shown in Figs. 7a,b.

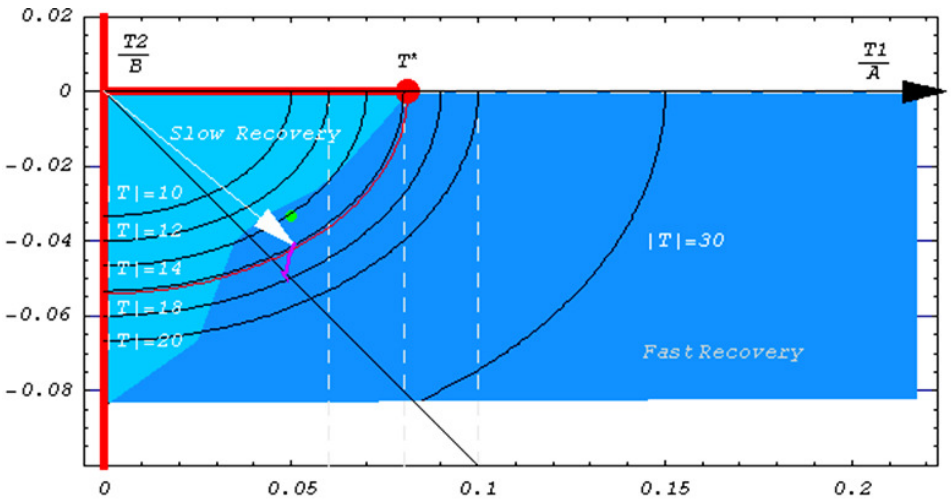

Figure 6 – Zoom of Part of Fig. 1; Green Dot: T = [10, -10]; |T| =14.14 Nm < T^* = 16.2203 Nm.

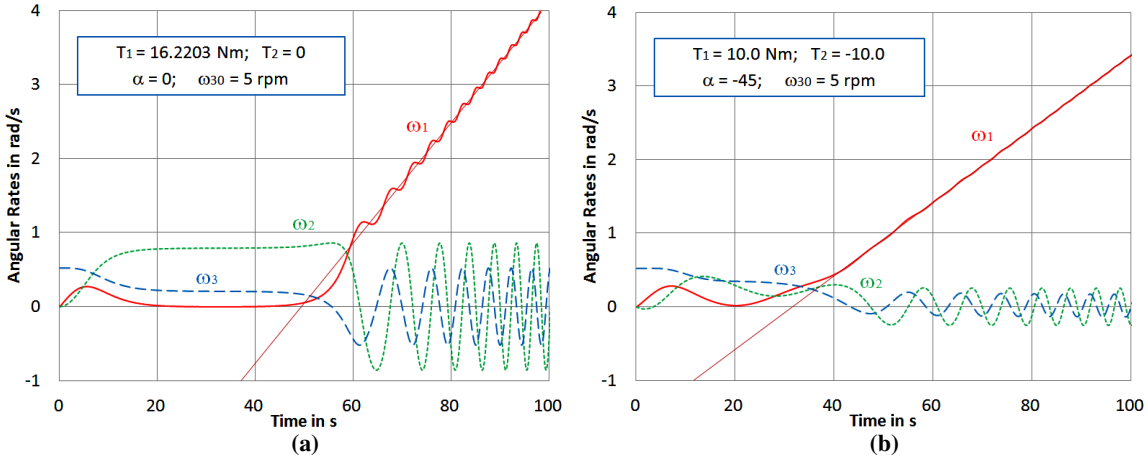

Figures 7 – a) $T_1 = T^* = 16.2203$; $T_2 = 0$; **b)** $T_1 = 10$; $T_2 = -10$ with $|T| = 14.14 < T^* = 16.2203$.

Table 1 – Comparison of Results for Torque Strategies of Figs. 7a,b.

	Fig. 7a: **T** = {T^*, 0}		Fig. 7b: **T** = {10 , -10}	
	times *t* (s)	**ω_1 (1/s)**	**times *t* (s)**	**ω_1 (1/s)**
1st Minimum ω_1	32.874	≈ 0	20.133	≈ 0.022
$\Delta E_{sep} = 0$	53.188	0.140	35.6	0.333
$\omega_3 = 0$	55.527	0.275	43.242	0.576
$\omega_2 = 0$	61.291	1.117	47.317	0.794
Linear $\omega_1(t_s) = 0$	t_s = 49.136 (s)		t_s = 31.365 (s)	
ΔE_{max} (initial)	54.831 Nm		54.831 Nm	
ΔE_{max} (final)	54.831 Nm		4.875 Nm	

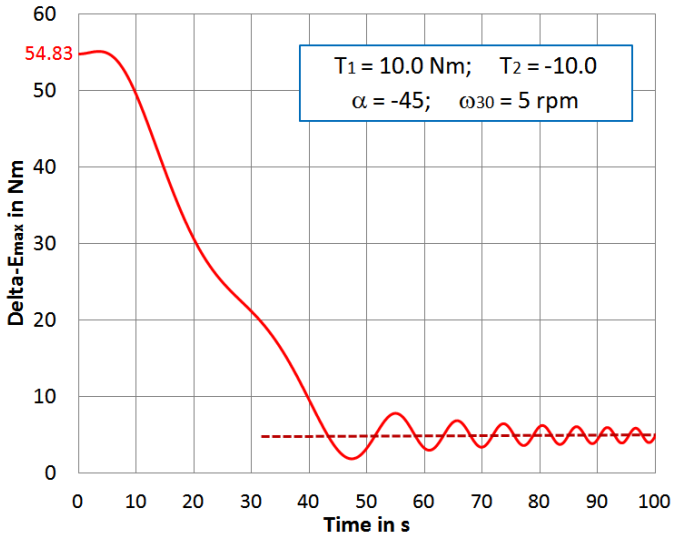

Figure 8 – Behavior of ΔE_{max} as Function of Time (Inputs as in Fig. 7b).

Table 2 shows the impact of the rotation angle α for torques of magnitude |**T**| = 16 Nm. When $\alpha = 0$ the torque is on the minimum (x) axis and the value of $-\alpha$ increases towards the negative intermediate axis ($-y$), i.e. it moves essentially on the red curve shown in Fig. 6.

Table 2 – Results for Different Rotation Angles α and Fixed Torque Magnitude of 16 Nm.

$-\alpha$	T_1	T_2	$t(\omega_1 = min)$	t_{sep}	$t(\omega_3 = 0)$	$\Delta E_{max}(\infty)$
deg	**Nm**		**s**			**Nm**
31.08	13.71	-8.25	14.85	17.55	21.41	~18
40	12.26	-10.28	16.61	20.86	25.71	~8
45	11.31	-11.31	17.96	24.28	30.79	3.5
50	10.28	-12.25	19.14	28.66	39.56	1.17
50.5	10.18	-12.35	19.23	29.10	40.42	1.135
51	10.07	-12.43	19.31	29.52	41.06	1.14
55	9.18	-13.01	19.75	32.81	43.03	2
60	8	-13.86	19.75	35.63	45.60	3.25
65	6.76	-14.5	19.65	39.91	53	2.2
70	5.47	-15.03	19.56	50.87	180	0.11

Table 2 shows that the time t_{sep} at which the separation plane is crossed and the time when ω_3 becomes zero always increase for increasing α. At the angle of 50.5° the asymptotic value of ΔE_{max} reaches its minimum on the red line segment starting from the white arrow in Fig. 6.

When α increases further to about 65°, the time to $\omega_3 = 0$ is comparable to the value in the case $T_2 = 0$ shown in Table 1. From this point onwards, the time to $\omega_3 = 0$ increases very rapidly for higher α angles, which is why we call this the '*Slow Recovery*' zone. The further evolution of ΔE_{max} is erratic within this zone, which is anyway of no practical interest for recovery strategies because of the increased recovery time.

APPROXIMATE ANALYTICAL RESULTS

Background and Objective

The highly non-linear Euler equations (see Eqs. 1,4) have many different types of solutions (for instance, periodic or a spin-up about the minimum or maximum axis of inertia), which cannot be described analytically by one formula. The different types of asymptotic motion have been summarized in the subsection Summary of Classifications.

The complexity of the solutions is also illustrated by the coefficients of a Taylor-series expansion which are provided (up to 6^{th} order) in Appendix A. For a single-axis torque, these series contain only even or odd terms. The coefficients depending on both torque components start only at 5^{th} order. The validity of these expansions over time is disappointing. Therefore, we present here approximate analytical results that are only valid in a restricted domain of the system parameters.

The numerical results in Figs. 7 show that, *after* the transition to a rotation about the minor x-axis, the angular velocity $\omega_1(t)$ has two distinct components. There is a *secular* term described by a *linear* function of time while the remaining part consists of increasingly fast *oscillations* about the linear trend line. The amplitude of these oscillations tends to a constant value. The right-hand side of Eq. (4a) shows that the slope of the secular term is m_1 and that the fast oscillations originate from the term $< k_1 \omega_2 \omega_3 >$. Figure 7 also shows that the $\{\omega_2, \omega_3\}$ rates describe fast oscillations about zero. The amplitudes of all fast oscillations tend to constant values.

Figs. 5 and 8 show that, after recovery, $\Delta E_{max}(t)$ fluctuates around a constant value with increasingly fast oscillations. The large change of $\Delta E_{max}(t)$ to its asymptotic value sets in before the transition. These observations are valid for any type of recovery.

The main objective of this section is to establish an approximate analytical model for $\Delta E_{max}(t)$ that provides insights into the asymptotic behavior of the residual nutation for $t \to \infty$.

New System of Equations Based on ΔE_{max}

Under an arbitrary equatorial torque the value of ΔE_{max} varies with time and the pair of rates $\{\omega_2, \omega_3\}$ moves on an ellipse with its origin at the center of mass, while the semi-axes have fixed directions but varying magnitudes $a(t)$ and $b(t)$:

$$\frac{\omega_2^2(t)}{a^2(t)} + \frac{\omega_3^2(t)}{b^2(t)} = 1 \tag{25}$$

Therefore, the rates $\{\omega_2, \omega_3\}$ may be expressed as:

$$\omega_2(t) = a(t) \sin \varphi(t); \quad \omega_3(t) = b(t) \cos \varphi(t) \tag{26a,b}$$

where $\varphi(t)$ is similar (apart from its origin on the semi-minor axis and its clockwise sense of rotation) to the eccentric anomaly of the *osculating* ellipse with varying semi-axes:

$$a(t) = \sqrt{\frac{2A}{BC} \frac{\Delta E_{max}(t)}{k_3}} \quad > \quad b(t) = \sqrt{\frac{2A}{BC} \frac{\Delta E_{max}(t)}{k_2}} \tag{27a,b}$$

From Eqs. (27) follows:

$$\Delta E_{max}(t) = \frac{BC}{2A} k_3 a^2(t) = \frac{BC}{2A} k_2 b^2(t) \tag{28a,b}$$

We introduce the new variable $\alpha(t)$ to replace the variables $a(t)$ and $b(t)$:

$$\alpha(t) = \sqrt{\frac{2A}{BC} \Delta E_{max}(t)} = \sqrt{k_3}\, a(t) = \sqrt{k_2}\, b(t) \tag{29a-c}$$

Thus, $\Delta E_{max}(t)$ is proportional to $\alpha^2(t)$ and has no explicit dependence on $\varphi(t)$.

By differentiating $\alpha^2(t)$ we obtain:

$$\alpha(t) \dot{\alpha}(t) = \frac{A}{BC} \frac{d}{dt} \{\Delta E_{max}(t)\} \tag{30}$$

For an equatorial torque vector we find from Eq. (21a):

$$\frac{A}{BC} \frac{d}{dt} \{\Delta E_{max}(t)\} = k_3 m_2 \omega_2(t) \tag{31}$$

Eqs. (30-31) along with Eq. (26a) lead to a compact equation for $\alpha(t)$:

$$\boxed{\dot{\alpha}(t) = m_2\sqrt{k_3}\,\sin\varphi(t)} \tag{32}$$

When substituting Eqs. (26) into the 2nd and 3rd Euler equations (i.e., Eqs. 4b,c) we find:

$$\boxed{\dot{\varphi}(t) = k_n\,\omega_1(t) + \frac{m_2\sqrt{k_3}}{\alpha(t)}\cos\varphi(t)} \tag{33}$$

with:

$$k_n = \sqrt{k_3\,k_2} = \sqrt{\frac{(B-A)(C-A)}{BC}} \tag{34}$$

For completeness sake, we also express the 1st Euler equation (i.e., Eq. 4a) in $\alpha(t)$ and $\varphi(t)$:

$$\boxed{\dot{\omega}_1(t) = m_1 - \frac{k_1}{2k_n}\alpha^2(t)\sin\{2\varphi(t)\}} \tag{35}$$

Because no simplifying assumptions have been made, the system of Eqs. (32-35) in terms of the variables $\alpha(t)$, $\varphi(t)$, and $\omega_1(t)$ is equivalent to the Euler equations in Eqs. (4) for an equatorial torque. We note that Eqs. (31-35) can be easily generalized for a torque with $m_3 \neq 0$.

Calculation of Point of Transition

If only the torque component m_1 is present, Eq. (33) reduces to:

$$\dot{\varphi}(t) = k_n\,\omega_1(t) = k_n\,\dot{u}(t) \quad with: \;\; u(t) = \int_0^t \omega_1(\tau)\,d\tau \tag{36a-c}$$

where u is the rotation angle about the minimum axis and φ is proportional to u (see Ref. 2). When comparing Eqs. (33) and (36a) we see that the presence of the torque m_2 increases the complexity of the problem since the variable u is no longer proportional to φ but:

$$k_n\,\dot{u}(t) = \dot{\varphi}(t) - \frac{m_2\sqrt{k_3}}{\alpha(t)}\cos\varphi(t) \tag{37}$$

The change to u as independent variable does no longer lead to an analytical solution in this case.

However, Eq. (22b) produces the only first integral of the present system (see also Ref. 1, Eq. 28a). When adopting u of Eq. (36b) as the independent variable we find from Eq. (22b):

$$\frac{d}{du}\left\{\Delta E_{sep}(u)\right\} = -\frac{AC}{B}k_3 m_1 \quad \Rightarrow \tag{38a}$$

$$\Delta E_{sep}(u) = \Delta E_{sep}(0) - \frac{AC}{B}k_3 m_1 u(t) \tag{38b}$$

When considering an initial *pure* flat-spin condition we can calculate $\Delta E_{sep}(0)$ from Eq. (20b):

$$\Delta E_{sep}(0) = \frac{AC}{2B}k_1\,\Omega_0^2 \tag{39}$$

The transition to a spin about the minimum axis occurs at $u = u^*$ with $\Delta E_{sep}(u^*) = 0$. The value u^* follows immediately from Eqs. (38b) and (39):

$$u^* = \frac{\Omega_0^2}{2m_1}\frac{k_1}{k_3} \tag{40}$$

Approximate Model for Fast Recoveries

After a recovery, the presence of the torque m_1 in Eq. (35) ensures that $\omega_1(t)$ continues to increase steadily. Since the 2nd term on the right-hand-side of Eq. (35) is a periodic function of φ, the slope of $\omega_1(t)$ will average to m_1. We assume here that this *averaged* evolution of $\omega_1(t)$, but not its instantaneous value, is valid from the start at $t = 0$. This assumption is applicable only in part of the "Fast Recovery" zone in Fig. 2. Thus, we introduce the averaged value of $\omega_1(t)$:

$$\tilde{\omega}_1(t) = <\omega_1(t)> = m_1 t \tag{41}$$

Similarly, by ignoring the periodic term in Eq. (33), we find the averaged evolution of $\varphi(t)$ as:

$$\tilde{\varphi}(t) = k_n \int_0^t \tilde{\omega}_1(\tau)\, d\tau = \frac{1}{2} k_n m_1 t^2 \tag{42}$$

After replacing the variable $\varphi(t)$ in Eq. (32) by its approximation in Eq. (42) we can integrate Eq. (32) and find the following approximate solution for $\alpha(t)$:

$$\tilde{\alpha}(t) = \alpha_0 + m_2 \sqrt{k_3} \int_0^t \sin\left(\frac{1}{2} k_n m_1 \tau^2\right) d\tau \tag{43}$$

which can be integrated (Ref. 16, p. 887) in terms of the Fresnel Sine Integral $S(t)$ as follows:

$$\tilde{\alpha}(t) = \Omega_0 \sqrt{k_2} + m_2 \sqrt{k_3} \sqrt{\frac{\pi}{k_n m_1}}\, S(t) \tag{44}$$

The result for α_0 follows from Eqs. (26b) and (29c) and corresponds to an initial pure flat-spin motion about the z-axis. The asymptotic value of the Fresnel Integrals $S(t)$ and $C(t)$ converges to 0.5 for $t \to \infty$ (Ref. 16, p. 890). Thus, the asymptotic value of Eq. (44) may be written as:

$$\tilde{\alpha}(\infty) = \Omega_0 \sqrt{k_2} \left\{ 1 + \frac{m_2}{2\Omega_0} \sqrt{\frac{k_3}{k_2}} \sqrt{\frac{\pi}{k_n m_1}} \right\} \tag{45}$$

We calculate the ratio:

$$\frac{\tilde{\alpha}(\infty)}{\alpha_0} = 1 + \varepsilon \quad with: \quad \varepsilon = \frac{\sqrt{\pi}}{2} \frac{\sqrt{k_n}}{k_2} \frac{\mu_2}{\sqrt{\mu_1}} \tag{46a,b}$$

with:

$$\mu_j = \frac{m_j}{\Omega_0^2} \quad (j = 1, 2) \tag{47a,b}$$

Finally, Eqs. (29a) and (46a) produce a compact asymptotic expression for ΔE_{max}:

$$\frac{\Delta E_{max}(\infty)}{\Delta E_{max}(0)} = \frac{\tilde{\alpha}^2(\infty)}{\alpha_0^2} = (1 + \varepsilon)^2 \tag{48}$$

In general, and in particular for "slow" recoveries, the linear model for $\tilde{\omega}_1(t)$ given by Eq. (41) is not valid and the analytical approach presented above should not be used. Appendix B provides a straightforward first-order perturbation approach on the basis of $\tilde{\omega}_1(t) = m_1 (t - t_0)$ that may be applied instead.

Discussion of Results

Figures 9a,b show the numerical and analytical results for the asymptotic value of $\Delta E_{max}(t)$ for the fixed torque components T_1 = 20 Nm and T_1 = 30 Nm, respectively. The component T_2 varies in the interval (-50,0) Nm in both cases. The 'numerical' curve gives the numerical integration results whereas the 'analytical' curve is the solution established in Eq. (48).

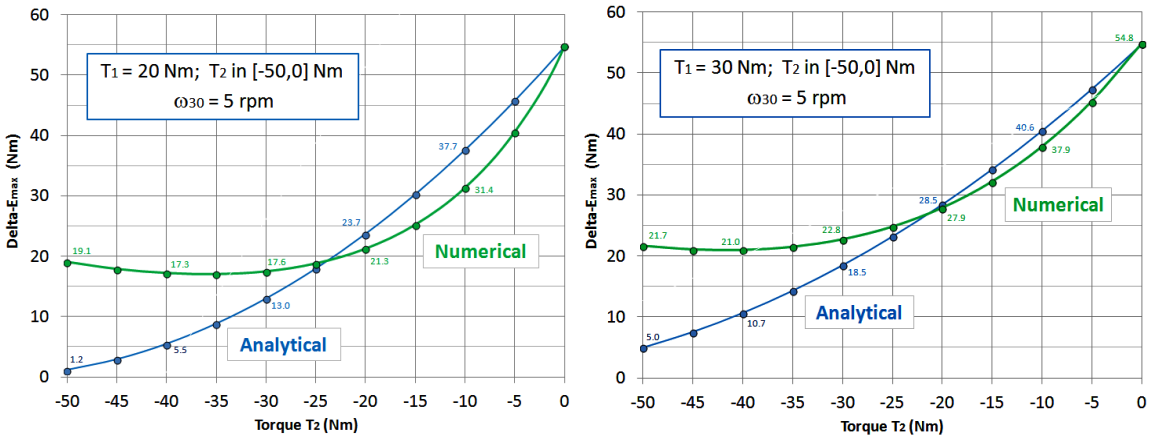

(a) T_1 = 20 Nm **(b) T_1 = 30 Nm**

Figures 9 – Numerical and Analytical Results for ΔE_{max} for Varying T_2 Component in Interval [-50,0] Nm.

The agreement between the analytical and numerical results is better in Fig. 9b than in Fig. 9a with average absolute differences of 5.5 versus 7.0. This may be understood from Fig. 6 where the circle of 30 Nm is well within the 'Fast-Recovery' zone whereas 20 Nm is close to the edge of this zone. For $T_2 > 0$ (not shown) we approach the border of the 'No Recovery' zone (see Figs. 2,6) so the comparisons in Figs. 9a,b diverge for increasing $T_2 > 0$ and ΔE_{max} approaches infinity.

Figures 10a,b show the numerical and analytical asymptotic results for ΔE_{max} for fixed torque magnitudes, i.e. $|\mathbf{T}|$ = 30 Nm (Fig. 10a) and $|\mathbf{T}|$ = 16 Nm (Fig. 10b), and a varying phase angle α within the interval (-70,0) deg. The difference between the results in Figs. 10a, 10b is remarkable with average absolute differences of 1.5 and 16.4 Nm, respectively. The torque magnitude $|\mathbf{T}|$ = 30 Nm in Fig. 10a is deep into the zone of 'fast recoveries', whereas $|\mathbf{T}|$ = 16 Nm in Fig. 10b lies on the red circle in Fig. 6. The numerical results between α = -50° and α = -60° are very erratic because this region is essentially on the border between the fast and slow recoveries, see Fig. 6.

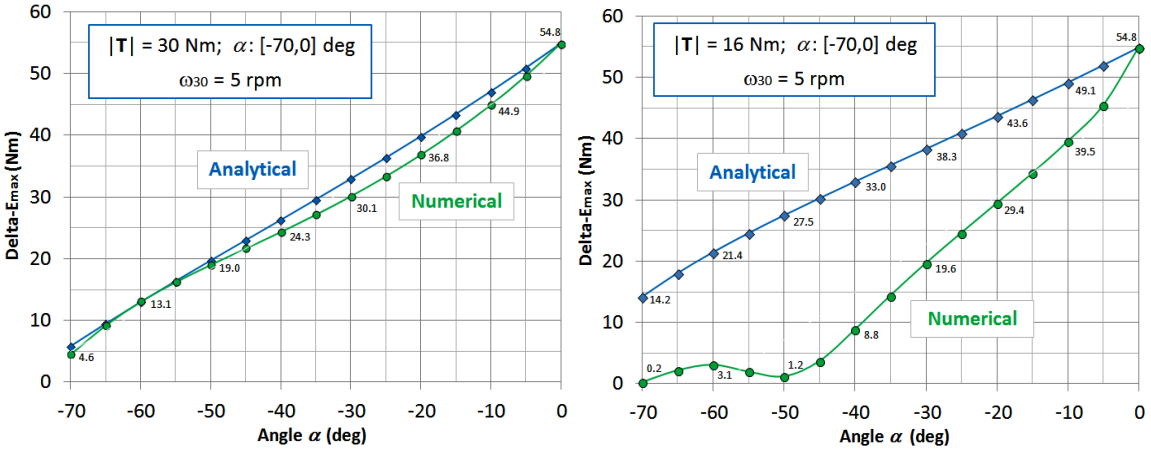

(a) |T| = 30 Nm **(b) |T| = 16 Nm**

Figures 10 – Analytical and Numerical Results for ΔE_{max} under Varying Torque Phase Angle α.

CONCLUSION

The results presented here provide new valuable and interesting insights into the motion of a spinning rigid asymmetric spacecraft under an equatorial torque. In particular, the findings have practical relevance in terms of a recovery from a flat-spin condition. Four classes of motion are identified and visualized as zones within the plane formed by the two equatorial torque components. Periodic solutions occur only for single-axis torques with x-axis torque component T_1 below a critical value T^* and for any T_2 component along the y-axis. The 'No Recovery' zone contains a new type of unstable motion. The zone 'Slow Flat-Spin Recovery' gives new insights into the efficiency of a recovery strategy by using an equatorial torque. The final class of motion is the 'Fast-Recovery' zone, where the recovery transition to a spin-up about the minimum axis of inertia takes place during the first revolution. Of particular interest is the part of the "Fast-Recovery" zone where $T_2 < 0$ and the modulus of the torque vector is below a critical value. Here, the flat-spin recovery is very efficient and the final nutation is relatively small. A new compact system of equations is derived for predicting the angular rates and the excess (or deficit) energy quantity ΔE_{max}. Approximate analytical results are presented for the asymptotic behavior of the rates as well as for ΔE_{max} in terms of the Fresnel Sine Integral. This leads to useful insights into the asymptotic behavior of the resulting recovery motion. The numerical and analytical results are illustrated through a number of Figures showing the feasibility and efficiency of the flat-spin recovery under different system parameters.

REFERENCES

1. F. L. Janssens and J. C. Van der Ha, "Flat-Spin Recovery of Spinning Satellites by an Equatorial Torque." *Acta Astronautica*. Vol. 116, November-December 2015, pp. 355-367. (doi:10.1016/ j.actaastro.2015.05.011)
2. F. L. Janssens and J. C. Van der Ha, "Analytical Solution for Flat-spin Recovery of Spinning Satellites." *Advances in the Astronautical Sciences, Space Flight Mechanics 2014*. Vol. 152, pp. 3495-3513.
3. U. T. Bödewadt, "Der Symmetrische Kreisel bei Zeitfester Drehkraft." *Mathematische Zeitschrift*. Vol. 55, pp. 310-320, 1952.
4. R. Grammel, "Die Stationären Bewegungen des Selbsterregten Kreisels und ihre Stabilität." *Ingenieur-Archiv*. Vol. XXI, No. 3, pp. 149-156, 1953.
5. R. Grammel, "Der Selbsterregten Unsymmetrische Kreisel." *Ingenieur-Archiv*. Vol. XXII, No. 2, pp. 73-97, 1954.
6. E. Leimanis, *The General Problem of the Motion of Coupled Rigid Bodies About a Fixed Point*. Springer, New York, 1965.
7. Ph. Boland and F. Janssens, "The GEOS-1 Dynamic Experiment." *ESA Journal*. Vol. 3, No. 3, July 1979, pp. 265-280.
8. J. C. Van der Ha, "Perturbation Solution of Attitude Motion under Body-Fixed Torques." *Acta Astronautica*. Vol. 12, No. 10, October 1985, pp. 861-869.
9. J. M. Longuski and P. Tsiotras, "Analytical Solutions for a Spinning Rigid Body Subject to Time-Varying Body-Fixed Torques - Part I Constant Axial Torques." *Transactions of ASME*. Vol. 60, December 1993, pp. 970-975.
10. P. M. Barba, N. Furumoto, and I. P. Leliakov, "Techniques for Flat-Spin Recovery of Spinning Satellites." *AIAA Guidance and Control Conference*. Key Biscayne, FL, AIAA Paper 73-859, August 20-22, 1973.
11. D. L. Cronin, "Flat-spin Recovery of a Rigid Asymmetric Spacecraft." *Journal of Guidance and Control*. Vol. 1, No. 4, July-August 1978, pp. 281-282.
12. R. Livneh and B. Wie, "New Results for an Asymmetric Rigid Body with Constant Body-Fixed Torques." *Journal of Guidance, Control, and Dynamics*. Vol. 20, No. 5, September-October 1997, pp. 873-881.
13. R. Livneh and B. Wie, "Asymmetric Body Spinning Motion with Energy Dissipation and Constant Body-Fixed Torques." *Journal of Guidance, Control, and Dynamics*. Vol. 22, No. 2, March-April 1999, pp. 322-328.
14. Z. R. Manchester, "Lyapunov-Based Control for Flat-Spin Recovery and Spin Inversion of Spin-Stabilized Satellites." *AIAA/AAS Astrodynamics Specialist Conference, AIAA Space Forum*. Long Beach, CA, Sept 13-16, 2016, Paper AIAA 2016-5644. (doi: 10.2514/6.2016-5644)

15. W.T. Thomson, *Introduction to Space Dynamics*. Dover Publications. 1961 / 1986, p. 126.
16. I. S. Gradshteyn and I. M. Rizin, *Table of Integrals, Series and Products*, *7th Edition*. Elsevier Academic Press Publications, Burlington, MA, USA, 2007.

APPENDIX A – TAYLOR-SERIES COEFFICIENTS FOR EQUATORIAL TORQUE

Here we provide the first 6 coefficients of a Taylor-series expansion in time t for the rotation rates $\omega_1(t)$, $\omega_2(t)$, $\omega_3(t)$ and for $\Delta E_{max}(t)$. These results follow from the Euler equations in Eqs. (4) with pure flat-spin initial conditions $\omega_{10} = \omega_{20} = 0$; $\omega_{30} \neq 0$.

$\omega_1(t)$:

$$m_1\, t - \frac{1}{2}\,(k1\, m_2\, \omega_{30})\, t^2 - \frac{1}{6}\left(k_1\, k_2\, m_1\, \omega_{30}^2\right) t^3 + \frac{1}{24}\, k_1^2\, k_2\, m_2\, \omega_{30}^3\, t^4 + \frac{1}{120}\, k_1\, m_1\left(8\, k_3\, m_2^2 + k_1\, k_2^2\, \omega_{30}^4\right) t^5 - \frac{1}{720}\left(k_1\, m_2\, \omega_{30}\left(-43\, k_2\, k_3\, m_1^2 + 15\, k_1\, k_3\, m_2^2 + k_1^2\, k_2^2\, \omega_{30}^4\right)\right) t^6 + O[t]^7 \tag{A.1}$$

$\omega_2(t)$:

$$m_2\, t + \frac{1}{2}\, k_2\, m_1\, \omega_{30}\, t^2 - \frac{1}{6}\left(k_1\, k_2\, m_2\, \omega_{30}^2\right) t^3 - \frac{1}{24}\left(k_1\, k_2^2\, m_1\, \omega_{30}^3\right) t^4 + \frac{1}{120}\, k_2\, m_2\left(-8\, k_3\, m_1^2 + k_1^2\, k_2\, \omega_{30}^4\right) t^5 + \frac{1}{720}\, k_2\, m_1\, \omega_{30}\left(-15\, k_2\, k_3\, m_1^2 + 43\, k_1\, k_3\, m_2^2 + k_1^2\, k_2^2\, \omega_{30}^4\right) t^6 + O[t]^7 \tag{A.2}$$

$\omega_3(t)$:

$$\omega_{30} - \frac{1}{3}\,(k_3\, m_1\, m_2)\, t^3 + \frac{1}{8}\left(-k_2\, k_3\, m_1^2\, \omega_{30} + k_1\, k_3\, m_2^2\, \omega_{30}\right) t^4 + \frac{7}{60}\, k_1\, k_2\, k_3\, m_1\, m_2\, \omega_{30}^2\, t^5 + \frac{1}{48}\left(k_1\, k_2^2\, k_3\, m_1^2\, \omega_{30}^3 - k_1^2\, k_2\, k_3\, m_2^2\, \omega_{30}^3\right) t^6 + O[t]^7 \tag{A.3}$$

$\Delta E_{max}(t)$:

$$\Delta E_{max}(0) + \frac{B\,C}{2\,A}\, k_3\, m_2\, t^2 \left\{ m_2 + \frac{1}{3}\, k_2\, m_1 \omega_{30}\, t - \frac{1}{12}\, k_1 k_2\, m_2\, {\omega_{30}}^2\, t^2 - \frac{1}{60}\, k_1 k_2^2\, m_1\, {\omega_{30}}^3\, t^3 + \frac{1}{360}\, k_2\, m_2\, t^4 ({\omega_{30}}^4\, k_1^2\, k_2 - 8 k_3\, m_1^2) \right\} \tag{A.4}$$

APPENDIX B – FIRST-ORDER PERTURBATION APPROACH

Here we present a straightforward perturbation technique by separating the steadily increasing secular terms from the bounded periodic terms for the system of Eqs. (32-35):

$$\alpha(t) = \alpha_0(t) + \delta_\alpha(t) \tag{B.1a}$$

$$\varphi(t) = \varphi_0(t) + \delta_\varphi(t); \quad \omega_1(t) = m_1(t - t_0) + \delta_1(t) \tag{B.1b,c}$$

The periodic $\delta_\alpha(t)$, $\delta_\varphi(t)$, $\delta_1(t)$ functions are proportional to m_j (j = 1,2) and are assumed to be relatively small corrections of the secular terms. The initial conditions are:

$$\alpha_0(t_0) = \Omega_0\sqrt{k_2}; \quad \varphi_0(t_0) = 0; \quad \omega_1(t_0) = 0 \tag{B.2a-c}$$

Eq. (B.2a) refers to the initial *pure* flat-spin motion with $\omega_3(t_0) = \Omega_0$. Naturally, all initial conditions $\delta_x(t_0)$, with $x = \alpha, \varphi, 1$, vanish as well.

The leading set of equations follows by substituting Eqs. (B.1) in Eqs. (32-35) and collecting the secular contributions:

$$\dot{\alpha}_0(t) = 0; \quad \dot{\omega}_1(t) = m_1; \quad \dot{\varphi}_0(t) = k_n\,\omega_1(t) \tag{B.3a-c}$$

This yields the secular solutions:

$$\alpha_0(t) = \Omega_0\sqrt{k_2} = constant; \quad \omega_1(t) = m_1(t - t_0) \tag{B.4a,b}$$

$$\dot{\varphi}_0(t) = k_n\,\omega_1(t) \quad \Rightarrow \quad \varphi_0(t) = \frac{1}{2}k_n m_1(t - t_0)^2 \tag{B.4c,d}$$

These expressions are consistent with the approximate results of Eqs. (41-42). The corresponding equations for the bounded periodic terms follow from Eqs. (32-35):

$$\dot{\delta}_\alpha(t) = m_2\sqrt{k_3}\,\sin\varphi_0(t) \tag{B.5a}$$

$$\dot{\delta}_\varphi(t) = \frac{m_2}{\alpha_0}\sqrt{k_3}\,\cos\varphi_0(t); \quad \dot{\delta}_1(t) = -\frac{k_1}{2k_n}\alpha_0\,\sin\{2\varphi_0(t)\} \tag{B.5b,c}$$

When substituting Eq. (B.4d) into Eq. (B.5a) and integrating we obtain:

$$\delta_\alpha(t) = m_2\sqrt{k_3}\int_{t_0}^{t}\sin\left\{\frac{1}{2}k_n m_1\left(\tau - t_0\right)^2\right\}d\tau =$$

$$= m_2\sqrt{k_3}\int_0^{t-t_0}\sin\left\{\frac{1}{2}k_n m_1\sigma^2\right\}d\sigma = m_2\sqrt{k_3}\sqrt{\frac{\pi}{k_n m_1}}\,S(t - t_0) \tag{B.6}$$

The approximate solution for $\alpha(t)$ follows by adding the results of Eqs. (B.2a) and (B.6):

$$\alpha(t) \cong \Omega_0\sqrt{k_2} + m_2\sqrt{k_3}\sqrt{\frac{\pi}{k_n m_1}}\,S(t - t_0) \tag{B.7}$$

After substituting the asymptotic result of the Fresnel Integral for $t \to \infty$ we find the same result for $\alpha(t)$ as given in Eqs. (45).

Obviously, Eqs. (B.5b,c) may be integrated and expressed in Fresnel Integrals similarly as was done for $\delta_\alpha(t)$ in Eq. (B.6). These results correspond to the periodic perturbations acting on top of the secular trends of $\varphi_0(t)$ and $\omega_1(t)$.